Accurate Estimation of Chromatic Dispersion for Non-Degenerate Phase-Sensitive Amplification

Shimpei Shimizu ⬤, *Member, IEEE*, Takushi Kazama ⬤, Takayuki Kobayashi ⬤, *Member, IEEE*, Takeshi Umeki, *Member, IEEE*, Koji Enbutsu ⬤, Ryoichi Kasahara ⬤, and Yutaka Miyamoto, *Member, IEEE*

Abstract—A phase-sensitive amplifier (PSA) has the potential of low-noise optical amplification and nonlinear phase noise mitigation. For PSA operation, the chromatic dispersion (CD) that causes gain ripple must be compensated before amplification. We propose an accurate CD estimation method for non-degenerate PSAs (ND-PSAs). We experimentally demonstrated its effectiveness by using periodically poled LiNbO$_3$ waveguides as amplification mediums. We first modified the conventional formula for the gain spectrum under residual CD conditions to be applicable to ND-PSAs by considering phase locking. We then experimentally described the effect of passband narrowing due to the gain ripple on the signal quality using a probabilistically shaped 64QAM signal. Furthermore, we applied the modified formula to CD estimation and compensation. As a result, accurate CD estimation on the sub-ps/nm order and gain-flattened spectrum over 3.5 THz were demonstrated with our method. We also propose a method for estimating residual CD from the gain variation among wavelength division multiplexing (WDM) channels. The possibility of adaptive compensation for CD was shown by carrying out WDM amplification.

Index Terms—Chromatic dispersion, optical fiber communication, phase-sensitive amplification.

I. INTRODUCTION

O PTICAL transport networks using wavelength division multiplexing (WDM) have been widely deployed. High-capacity transmission has been demonstrated using higher-order modulation formats and additional transmission bands [1]. The multi-level of the modulation is restricted by the optical signal-to-noise ratio (OSNR). Therefore, it is important to enhance the OSNR for improving transmission capacity with more advanced modulation formats. In repeated-amplification transmission, the OSNR is restricted by the fiber loss and the noise figure (NF) of optical amplifiers. The NF is determined from the amount of amplified spontaneous emission (ASE) noise from optical

amplifiers. Typical amplifiers, such as erbium-doped fiber amplifiers (EDFAs) and Raman amplifiers, are classified as phase-insensitive amplifiers (PIAs). The NF of PIAs is always more than 3 dB due to the standard quantum limit (SQL) [2]. To relatively suppress the ASE noise, it is effective to enhance the fiber-input power of the signal light. However, the increase in input power causes waveform distortion due to unwanted nonlinear optical effects in fibers [3].

Toward further high-capacity optical networks, phase-sensitive amplifiers (PSAs) have attracted much attention because of their potential for low-noise amplification [4] and nonlinear phase noise mitigation including self-phase and cross-phase modulation [5]–[7]. Phase-sensitive amplification is carried out by optical parametric amplification (OPA) in nonlinear mediums, such as periodically poled LiNbO$_3$ (PPLN) [8], [9] and highly nonlinear fiber (HNLF) [10], [11], and can theoretically achieve an NF of 0 dB by amplifying only one of the quadrature phase components of the input light. There are two types of PSAs depending on the difference in frequency relation between the signal and idler lights (phase-conjugated signal lights), namely degenerate PSAs (D-PSAs) and non-degenerate PSAs (ND-PSAs). In a D-PSA, the input light to the amplifier is only the signal light, and the idler light at the same frequency as the signal is generated in the amplification medium. A D-PSA can typically be applied to single-channel amplification at the degenerate frequency and 1-bit modulation format such as BPSK. On the other hand, an ND-PSA requires both the signal and idler lights at different frequencies as the input lights to the amplifier. An ND-PSA can be applied for multichannel signals [12] and arbitrary modulation formats involving higher-order QAM [13]. Therefore, an ND-PSA has high affinity to WDM transmission systems with advanced modulation formats. An ND-PSA requires idler lights co-propagating with signal lights in transmission fibers. Thus, the effective NF of ND-PSAs can reach -3 dB because of the frequency-diversity effect. Recently, WDM amplification and an SNR advantage of around 5 dB compared with EDFAs have been demonstrated using PPLN waveguides and HNLFs [14]–[16]. The potential of ND-PSAs as inline amplifiers has also been demonstrated [17].

One of the most important problems we face in actual PSAs is the effect of chromatic dispersion (CD) on the gain spectrum. CD causes phase variation of signals in the frequency domain. This phase variation induces gain ripple because the gain of PSAs depends on the phase relation between signal and pump lights. Thus, CD generated in transmission fibers and optical

components needs to be compensated to enable phase-sensitive amplification. In previous studies, CD was compensated using dispersion compensating modules (DCMs) such as dispersion-compensating fibers and fiber-Bragg gratings [14], [15], [17]. However, it is necessary to provide more accurate CD compensation for wideband phase-sensitive amplification. As mentioned above, CD tolerance and accurate compensation are important factors in designing a transmission system using PSAs. CD tolerance in a D-PSA has been investigated [18]. Although that in an ND-PSA was also reported [19], the impact of CD during propagation in transmission fibers after idler generation has not been studied in detail. In a transmission system using PSAs as inline amplifiers, the residual CD during co-propagation with idlers determines the gain characteristic.

In our previous work, we investigated the impact of residual CD on signal quality and proposed a method estimating the residual CD from gain spectrum of ASE light [20]. In this paper, we discuss that work in more detail regarding the correspondence between theory and experiment and propose another CD estimation method using gain variation among WDM channels. This method can adaptively track CD variation due to environmental factors such as temperature fluctuation. Both methods target a slight residual CD which cannot be completely compensated with conventional methods. We conducted experiments to evaluate its effectiveness by using PPLN-based OPA modules. These methods are described by theoretically defining the effect of residual CD on ND-PSAs. In Section II, we present the theoretical gain ripple of an ND-PSA by modifying the conventional formula for D-PSAs under residual CD conditions. In Section III, we experimentally describe the effect of passband narrowing due to gain ripple on the signal quality using an advanced modulation format, probabilistically shaped 64QAM (PS-64QAM), with two symbol rates of 5 and 20 Gbaud. In Section IV, we present and experimentally demonstrate our method estimating residual CD by measuring the gain spectrum of PSAs. We also present residual CD estimation method using the gain variation among WDM channels toward adaptive CD compensation. We conducted a fundamental demonstration of this proposed method through an WDM-amplification experiment and show the detailed characteristics of estimation accuracy through numerical simulations.

II. GAIN SPECTRUM OF NON-DEGENERATE PSA

For accurate CD estimation, it is important to clarify the gain characteristics of PSAs with respect to CD. The operation of PSA requires phase locking between pump and signal lights. The conventional gain-spectrum formula for D-PSAs cannot be applied to ND-PSAs due to this phase locking. In this section, we describe the difference in gain spectrum between D-PSAs and ND-PSAs, and derive the theoretical gain spectrum of ND-PSAs under residual CD.

A. Theoretical Gain Spectrum Considering Phase Locking

The gain of PSAs G depends on the phase difference $\Delta\phi$ between the input and pump lights [21]:

$$G = G_I \cos^2(\Delta\phi) + \frac{1}{G_I}\sin^2(\Delta\phi), \quad (1)$$

where G_I is the gain of in-phase components, which means the maximum gain of the PSA. The gain repeats amplification and de-amplification every $\Delta\phi$ of $\pi/2$. For the phase-sensitive amplification of the signal, $\Delta\phi$ must be adequately controlled using a phase locking loop (PLL).

Under residual CD, $\Delta\phi$ depends on frequency. Therefore, the gain also depends on frequency, resulting in gain ripple. The rippled gain spectrum $G_{sp}(f)$ is expressed as [18]

$$G_{sp}(f) = G_I \cos^2[\Delta\phi(f)] + \frac{1}{G_I}\sin^2[\Delta\phi(f)]. \quad (2)$$

Ignoring the 3rd and higher order dispersion term, $\Delta\phi(f)$ is expressed as

$$\Delta\phi(f) = \frac{\pi Dc}{f_0^2}(f - f_0)^2, \quad (3)$$

where D is the residual CD affecting the gain characteristics, c is the velocity of light, and f_0 is the fundamental frequency in the phase-matching of the amplification medium and is the center frequency of the signal in a D-PSA. Each frequency component after a PSA has the same phase as the pump light thanks to phase regeneration of the PSA. Therefore, the residual CD, which affects the amplification characteristics, means the CD between PSA repeaters. Equation (2) is based on the assumption that $\Delta\phi(f_0) = n\pi$ (n is an integer). This assumption is correct in the case of D-PSAs because a PLL is used for maximizing the gain of the signal component at f_0 by adjusting the relative phase between the signal and pump lights. However, in an ND-PSA, the PLL monitors the signal-frequency component differently from f_0. Therefore, we modify the gain-spectrum formula to also support ND-PSAs by considering the PLL operation. Note that, for simultaneous amplification of WDM signals, a PLL requires the monitoring of only one arbitrary channel because the optical phase conjugator (OPC) for idler creation ensures that all signal-idler pairs have the same phase relations.

A PLL maximizes the gain of a monitored channel; thus, $\Delta\phi = n\pi$ at the PLL-target frequency f_{PLL}. Under this assumption, the gain spectrum is modified as

$$G_{sp}(f) = G_I \cos^2[\Delta\phi(f) - \theta] + \frac{1}{G_I}\sin^2[\Delta\phi(f) - \theta], \quad (4)$$

$$\theta = \frac{\pi Dc}{f_0^2}\Delta f^2, \quad (5)$$

where Δf is the bandwidth between f_0 and f_{PLL}. For example, Fig. 1 shows the gain spectrum calculated using Eqs. (2) and (4) with $G_I = 20$ dB, $f_0 = 193.0$ THz, and $D = 0.7$ ps/nm. The cases of $f_{PLL} = 193.0$ THz (D-PSA scheme) and $f_{PLL} = 193.5$ THz (ND-PSA scheme) are shown in Figs. 1 (a) and (b), respectively. It was confirmed that the gain spectrum in an ND-PSA differs from that in a D-PSA because of the difference in f_{PLL}. The 193.5-THz component is amplified at a 20-dB gain in an ND-PSA but not in a D-PSA. The f_{PLL} component is always amplified at G_I regardless of the amount of residual CD because of PLL operation.

B. Experimental Validation

To validate Eq. (4), we measured the gain spectrum of a PSA in two cases, i.e., continuous wave (CW) light at f_1 (193.0 THz) and at f_2 (194.0 THz), as the monitored channels of the PLL.
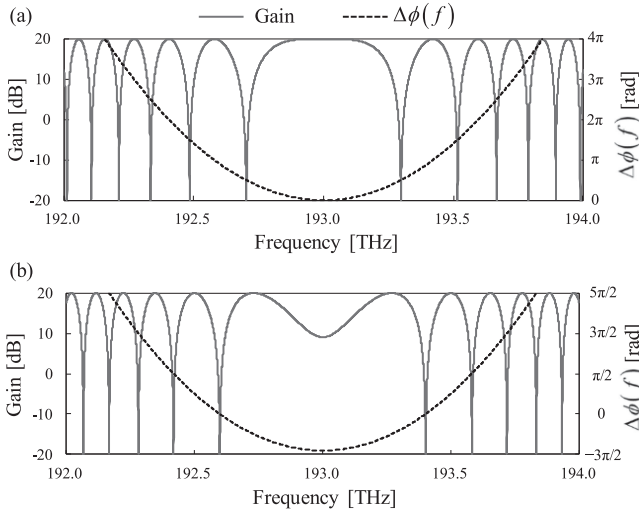
Fig. 1.   Gain spectra of PSAs with $G_{in} = 20$ dB, $f_0 = 193.0$ THz, and $D = 0.7$ ps/nm. (a) D-PSA ($f_{PLL} = 193.0$ THz). (b) ND-PSA ($f_{PLL} = 193.5$ THz).

The f_0 of the nonlinear mediums was 193.0 THz ($=f_1$); hence, the amplification for $f_{PLL} = f_1$ was carried out for the D-PSA. Fig. 2 shows the experimental setup. To measure the broad gain spectrum of a PSA, we used ASE light having symmetric phase-conjugated correlation as input to the PSA. PPLN waveguides were used as nonlinear mediums. The detailed operation of each module is described in a previous study [22]. The OPC stage generated the idler in PPLN1 by using a second harmonics (SH) pump. The SH pump was generated from a local oscillator (LO1) at 193.0 THz by SH generation (SHG) in the PPLN2. The OPC also generated ASE light simultaneously, and this ASE light had symmetric phase-conjugated correlation centered on f_0, like a signal-idler pair. The light then passed through a 20-m polarization-maintaining fiber (PMF), which acted as a dispersion medium, and was input to the PSA stage. The SH pump for the PSA was generated using LO2 and PPLN4, as with the OPC stage. The carrier recovery and frequency locking of LO2 were carried out using a sum-frequency-generation- (SFG-) assisted optical PLL (OPLL) [23]. We used a piezoelectric-transducer-based PLL (PZT-PLL) to compensate for the relative phase drifts between the signal and SH pump. The PZT-PLL monitored the power of the output signal at f_{PLL} extracted with a band-pass filter (BPF) with 60-GHz bandwidth and maximized the measured power by controlling the relative phase. The OPLL and PZT-PLL used the signal light tapped using a 10% coupler. The gain of the PSA was 23 dB, and the output spectrum was observed using the optical spectrum analyzer (OSA) with 0.1-nm resolution. The amplified ASE spectrum corresponded to the gain spectrum of the PSA because each frequency component in the ASE was phase-sensitive amplified thanks to symmetric phase correlation.

Fig. 3 shows the spectrum after the OPC stage in the ND-PSA scheme. The ASE spectrum monotonically increased by about 0.5 dB from 191.2 to 194.8 THz. Signal and idler were almost the same power of −6.0 dBm, and the ASE floor was −52.5 dBm around 193.0 THz, on the OSA. Fig. 4 shows the measured spectra after a D-PSA and an ND-PSA. The gain ripple

caused by residual CD was confirmed. The residual CD in this setup was estimated to be 0.68 ps/nm by comparing the output spectrum in the D-PSA scheme and conventional formula, Eq. (2) [Fig. 3(a)]. By deforming Eq. (2), the residual CD affecting the gain spectrum can be expressed as

$$D = \frac{f_0^2}{cB^2},\qquad(6)$$

where B is the bandwidth between f_0 and first peak ($\Delta\phi = \pi$) of gain spectrum in a D-PSA. The gain spectrum in the case of phase locking for f_2 was in good agreement with the theoretical spectrum calculated using the modified formula, i.e., Eq. (4), with 0.68-ps/nm CD [Fig. 4(b)]. Thus, it was confirmed that Eq. (4) is a generalized formula for the gain spectrum of PSAs considering PLL operation.

III. Impact of Residual CD on Signal Quality

As described above, the channel at f_{PLL} is always amplified regardless of residual CD thanks to the PLL. However, the signal quality is degraded due to passband narrowing if the bandwidth of the gain spectrum around f_{PLL} is narrower than the signal bandwidth. The signal bandwidth and gain bandwidth depend on the symbol rate and Δf, respectively. We experimentally investigated that the CD tolerance in an ND-PSA for a single channel depends on the symbol rate and Δf.

The configurations of the OPC and PSA stages were the same as the setup in Fig. 2. The CW light was modulated to single-polarized PS-64QAM with entropy of 5.0 bits by using an I-Q modulator (IQM). The roll-off factor of Nyquist spectral shaping was 0.1. The symbol rates were set to 20 and 5 Gbaud, and the center frequencies of the channels were 194.0 and 193.1 THz, at which Δf were 1 THz and 100 GHz, respectively. The residual CDs were induced using cascaded PMFs with various lengths and were varied between 0.92–11.58 ps/nm. The residual CD of each setup was measured using Eq. (6) for the D-PSA with a CW light. The OSNR at the output of the PSA was adjusted to about 23 dB regardless of PMF lengths and symbol rates by using a variable optical attenuator (VOA). The output signals were received using a coherent receiver and demodulated offline using a data-aided algorithm, and signal qualities were evaluated using normalized generalized mutual information (NGMI). We also conducted numerical simulations for each experimental condition.

Fig. 5 shows the NGMI dependence on residual CD, symbol rates, and Δf. At 194.0 THz, the 20-Gbaud signal rapidly degraded from about 2 ps/nm, and its constellation with a 3.17-ps/nm CD was unclear from inter-symbol interference due to passband narrowing. The tolerance with an NGMI penalty of 0.1 was enhanced to about 9 ps/nm for the 5-Gbaud signal because of its narrower bandwidth. The 193.1-THz channel had high CD tolerance because its frequency was in a band with gradual gain variation. The experimental results almost corresponded to the simulation results but were worse because the PLL was unstable due to passband narrowing. These results indicate that, for single-channel transmission, more accurate CD compensation is required for a high symbol-rate signal, and the channel frequency should be close to f_0.
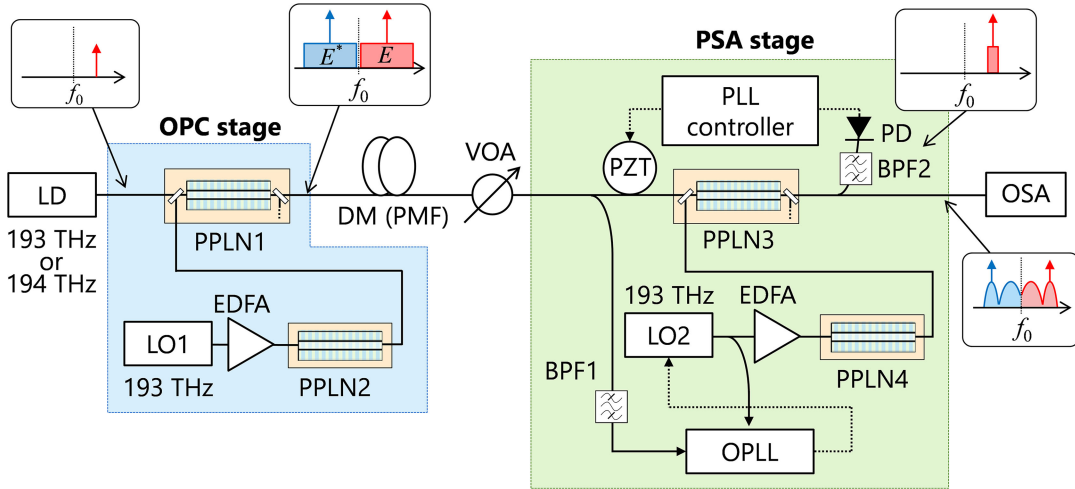
Fig. 2. Experimental setup for measuring gain spectrum; LD: laser diode, LO: local oscillator, DM: dispersion medium, PMF: polarization-maintaining fiber, BPF: band-pass filter, PZT: piezoelectric transducer, OPLL: optical PLL, PD: photodiode, OSA: optical spectrum analyzer.
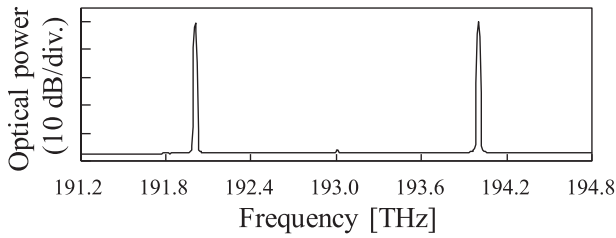

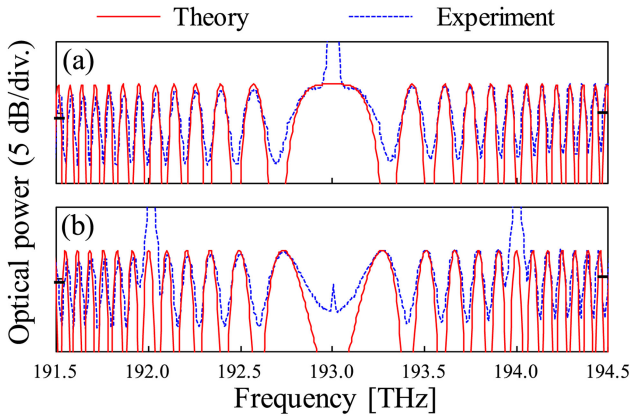Fig. 3. Spectrum after OPC stage in ND-PSA scheme.

Fig. 4. Experimental spectra and theoretical gain spectra with 0.68-ps/nm CD. Prominent peaks indicate input CW light and its idler light for PLL operation. (a) D-PSA scheme. (b) ND-PSA scheme.

Fig. 6 shows the amplified spectra for 20- and 5-Gbaud signal at 194.0 THz under residual CD conditions. Theoretical gain spectra are also shown in these figures. The signal spectra with 0.92-ps/nm CD indicated the transmit spectra [Fig. 6(a), (d)]. The 20-Gbaud signal with 2.81-ps/nm CD was affected by pass-band narrowing which is the 3-dB bandwidth of about 11 GHz, and gained a large NGMI penalty of about 0.2 [Fig. 6(b)]. On the other hand, the 5-Gbaud signal with the same CD was maintained the transmit spectrum [Fig. 6(e)]. The 20-Gbaud signal with 8.07-ps/nm CD was shaped in the form of a gain ripple, and the
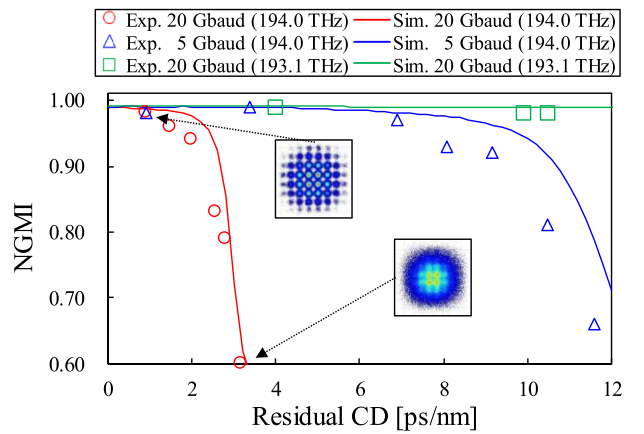

Fig. 5. NGMI as function of residual CD for each symbol rate and Δf. Plots and lines indicate experimental and simulation results, respectively. Constellations are for 0.92- and 3.17-ps/nm CD in 20-Gbaud signal at 194.0 THz.

5-Gbaud signal with the same CD was also affected by passband narrowing [Fig. 6(c), (f)]. The signal spectra with passband narrowing were in good agreement with forms of theoretical gain spectra under corresponding CD conditions in all cases.

IV. CD ESTIMATION METHOD FROM GAIN CHARACTERISTICS

Flat bandwidth in the gain spectrum is important for simultaneous amplification of wideband WDM signals. To extend the amplification bandwidth, residual CD must be accurately estimated and compensated. However, CD estimation is difficult because the CD affecting the gain spectrum is a partial CD between PSA repeaters and must be compensated for every repeater. This is because the output signal from PSAs does not have phase variation in the frequency domain due to the phase regeneration of PSAs. Moreover, compensation accuracy degrades if the points of CD estimation and amplification are different. The compensation accuracy requires a sub-ps/nm order as mentioned above. In this section, we present our proposed methods of estimating residual CD accurately by measuring the
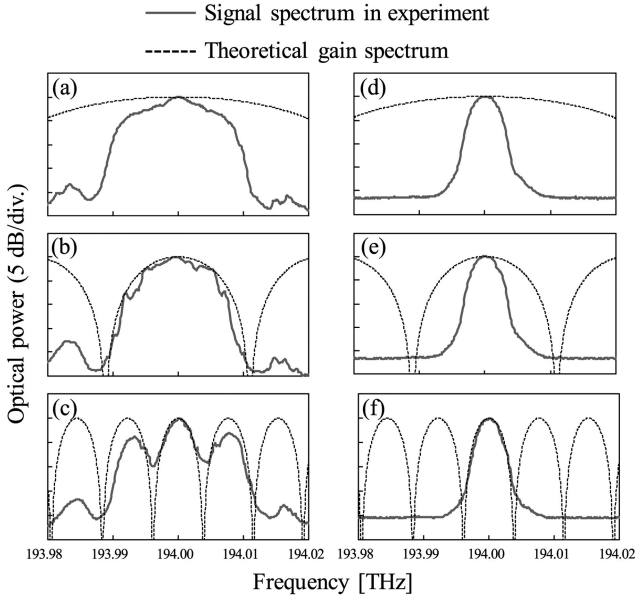
Fig. 6. Spectra of amplified signal 1-THz away from f_0. and theoretical gain spectra. (a) 20-Gbaud signal with 0.92-ps/nm CD. (b) 20-Gbaud signal with 2.81-ps/nm CD. (c) 20-Gbaud signal with 8.07-ps/nm CD. (d) 5-Gbaud signal with 0.92-ps/nm CD. (e) 5-Gbaud signal with 2.81-ps/nm CD. (f) 5-Gbaud signal with 8.07-ps/nm CD.
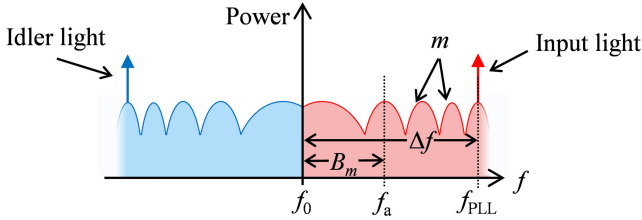

Fig. 7. Diagram of proposed CD estimation method in measured gain spectrum.

gain characteristics. The variation in PSA gain is very sensitive to CD. Therefore, only CD that actually affects amplification can be accurately estimated by comparing the obtained gain characteristics and theoretical formula, i.e., Eq. (4). With our methods, it is assumed that large CD is compensated up to ps/nm by the dispersion-compensating optical link, and a slight residual CD is targeted.

A. CD Estimation From Gain Spectrum

Residual CD from gain spectrum can be estimated by measuring marked frequencies such as peaks in the gain spectrum. We discussed our method of residual CD estimation for D-PSAs by measuring the peak in Section II. In this subsection, we expand this estimation method for any PSA, including ND-PSA by deforming Eq. (4). Fig. 7 shows a diagram of this method. Considering PLL operation, the phase at frequencies of the peaks in the gain spectrum indicate that $\Delta\phi(f) - \theta = n\pi$ (n is an integer). By using the bandwidth B_m between the arbitral peak at f_a and f_0, the residual CD is calculated as

$$D = \frac{f_0^2}{c\left(B_m^2 - \Delta f^2\right)}\left(m + 1\right),\qquad(7)$$
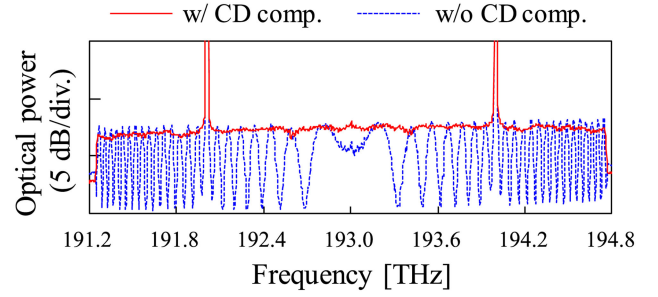

Fig. 8. Measured gain spectra with and without CD compensation.

where m is the number of peaks between the peaks at f_{PLL} and f_a. The phase difference between components at f_a and f_{PLL} is $(m + 1)\pi$. For simplicity, we ignored 3rd and higher order CD. If the 3rd-order CD strongly affects PSA performance and needs to be compensated, it can be calculated as the slope of 2nd-order residual CD estimated using some peaks in the gain spectrum.

To evaluate this method, we conducted an experiment on CD compensation. The gain spectrum was obtained using the same method and setup described in Section II. The frequency of the CW was set to 194.0 THz ($=f_{\mathrm{PLL}}$). We compensated for residual CD by phase modulation in the frequency domain with an optical programmable filter based on spatial light modulator (SLM) after the OPC stage. The SLM modulated the phase of input light in frequency domain, and its resolution was 0.1 GHz. The CD control range of the SLM was -25 to $+25$ ps. The amount of phase modulation fed back to the SLM at each frequency was calculated according to the estimated CD. Fig. 8 shows the measured spectra with and without CD compensation of 0.92 ps/nm. We used the peak around 193.57 THz ($m = 4$) for the CD estimation. With different m from 0 to 6, CD was estimated to be 0.92 ± 0.005 ps/nm. By CD compensation, the flat gain spectrum within 1 dB was observed over 3.5 THz, which was the bandwidth of the SLM. From this spectrum and Eq. (4), the compensation reduced the residual CD to less than 0.02 ps/nm. This result suggests that broad WDM amplification can be attained by estimating residual CD, which affects PSA gain, then compensating for it on the order of sub-ps/nm. Note that, a highly resolved spectrum will be needed for estimating higher CD because the ripple becomes finer.

We also carried out simultaneous amplification of 10-WDM channels, which were in a 100-GHz grid in the range of 193.1–194.0 THz, with CD compensation. The experimental setup is shown in Fig. 9. The 10-WDM CW lights were modulated to single-polarized 20-Gbaud PS-64QAM by using an IQM. The input power to the PSA was set to -35 dBm per channel. The signals were tapped using a 10% coupler before the PSA stage, and Ch. 1 at 193.1 THz and its idler channel at 192.9 THz were extracted using BPF1 for SFG-assisted OPLL. The signals were also tapped after the PSA stage, and Ch. 1 was extracted using BPF2 for PZT-PLL. In an ideal situation without residual CD, phase locking can be carried out by monitoring one arbitrary channel because signal-idler pairs are simultaneously generated by shared pump light in the OPC stage. The demodulation target channel was selectively extracted from amplified WDM signals by using BPF3. The residual CD was 0.92 ps/nm because
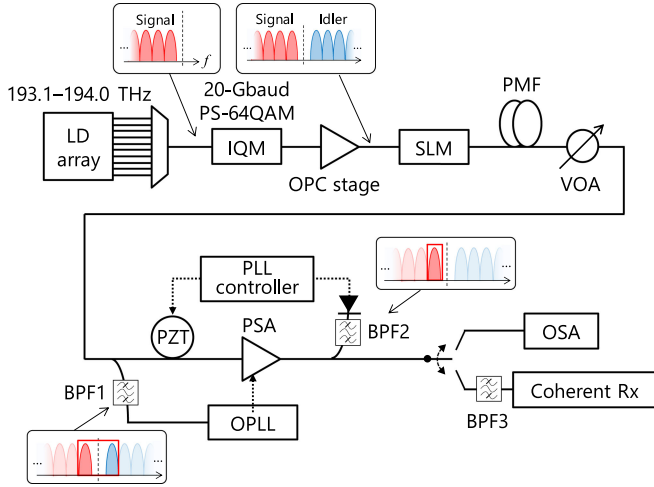
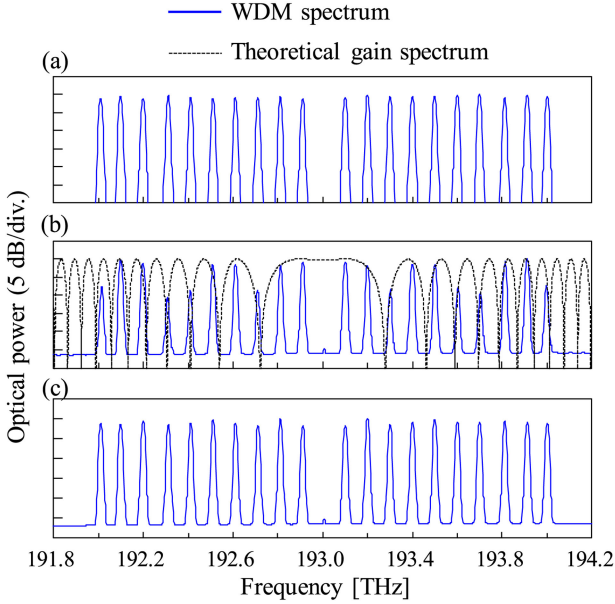Fig. 9. Experimental setup for WDM amplification.

Fig. 10. WDM spectra with 20-Gbaud PS-64QAM. (a) PSA-input spectrum. (b) Amplified spectrum and theoretical gain spectrum without CD compensation. (c) Amplified spectrum with CD compensation using value estimated from gain spectrum.

the setup from the OPC stage to the PSA stage was the same configuration as in the experiment in previous paragraph.

Fig. 10 shows the input and output spectra of a PSA with and without CD compensation. The spectrum variation among the input WDM signals was within 1.3 dB [Fig. 10(a)]. In the amplified spectrum without CD compensation, a gain difference larger than 10 dB was observed, and the gain variation was in good agreement with the form of theoretical gain spectrum calculated using Eq. (4) [Fig. 10(b)]. The spectrum variation was suppressed to within 2 dB by compensating for CD [Fig. 10(c)]. Fig. 11 shows the channel dependence of the NGMI. Several channels maintained good quality while gain ripple degraded other channels in the case of without CD compensation. Although Ch. 8 at 193.8 THz appeared to be strongly amplified, its NGMI degraded due to passband narrowing. Although Ch. 9 at
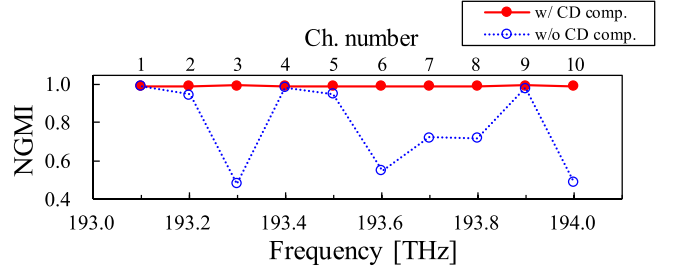

Fig. 11. NGMI characteristics for each channel.

193.9 THz was also allocated near the edge of the passband, it was confirmed that passband narrowing did not occur according to the NGMI characteristics. This is because Ch. 9 was closer to the center of the passband than Ch. 8. Meanwhile, flat NGMI performance was achieved across all channels by compensating for residual CD using the proposed CD estimation method. It was confirmed that wideband WDM amplification without signal deterioration is possible by accurately estimating and compensating for residual CD.

B. CD Estimation From Gain Variation Among WDM Channels

To compensate for CD constantly, adaptive compensation is necessary because CD varies with the environment of the fiber such along with temperature [24]. Although the variation of CD due to temperature variation is slight, it can generate a significant gain ripple in PSAs. Therefore, CD monitoring is required in service. However, the method described in Section IV-A is unstable for real-time monitoring since it requires a broad ASE light for CD estimation. In this subsection, we discuss our other proposed CD estimation method using the gain variation among WDM channels. The gain of each channel can be obtained by measuring the input and output powers of PSAs. A PSA supported by PLLs requires tapping signals before and after amplification for synchronization between signals and a pump light. Therefore, PSA gain measurement can be implemented naturally.

This method uses the gain ratio G_R among WDM channels. The G_R is expressed as

$$G_R \equiv \frac{G_a}{G_{PLL}}, \tag{8}$$

where G_{PLL} and G_a are the gain of the channel at f_{PLL} and an arbitral channel at f_a, respectively. The G_{PLL} and G_a are expressed as

$$G_{PLL} = G_I, \tag{9}$$

$$G_a = G_I \cos^2\left[\Delta\phi\left(f_a\right) - \theta\right] + \frac{1}{G_I}\sin^2\left[\Delta\phi\left(f_a\right) - \theta\right], \tag{10}$$

respectively. Therefore, G_R is calculated as

$$G_R = \frac{G_I^2 + 1}{2G_I^2} + \frac{G_I^2 - 1}{2G_I^2}\cos\left[\frac{2\pi Dc}{f_0^2}\left(\Delta f_a^2 - \Delta f^2\right)\right], \tag{11}$$
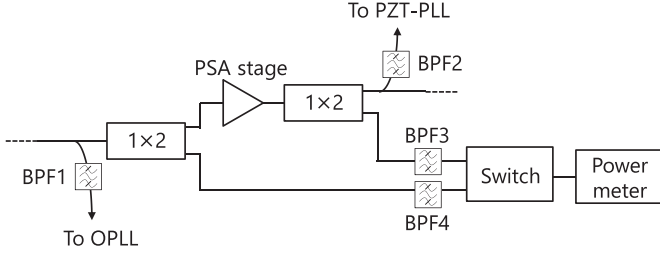
Fig. 12. PSA-stage configuration in experimental setup for demonstration of CD estimation method using gain difference among WDM channels.

where $\Delta f_{\mathrm{a}} = f_{\mathrm{a}} - f_0$. Thus, by deforming Eq. (11), residual CD can be estimated as

$$D = \frac{f_0^2}{2\pi c \left(\Delta f_{\mathrm{a}}^2 - \Delta f^2\right)} \cos^{-1}\left[\frac{\left(2G_{\mathrm{R}} - 1\right) G_{\mathrm{I}}^2 - 1}{G_{\mathrm{I}}^2 - 1}\right].$$

$$\approx \frac{f_0^2}{2\pi c \left(\Delta f_{\mathrm{a}}^2 - \Delta f^2\right)} \cos^{-1}\left(2G_{\mathrm{R}} - 1\right) \; (G_{\mathrm{I}} \gg 1) \quad (12)$$

Moreover, from the range of cosines, the measurement range is expressed as

$$D^2 < \frac{f_0^4}{4c^2 (\Delta f_{\mathrm{a}}^2 - \Delta f^2)^2}. \quad (13)$$

The closer f_{a} is to f_{PLL}, the larger the measurement range becomes. The monitored G_{R} becomes 1 by CD compensation based on the estimated CD when the residual CD is within the measurement range. If the residual CD exceeds the measurement range, the estimated value is incorrect and compensation is not carried out correctly. Thus, G_{R} after CD compensation does not become 1. In this case, the amount of residual CD is represented as

$$D = \frac{f_0^2}{2\pi c \left(\Delta f_{\mathrm{a}}^2 - \Delta f^2\right)} \left\{\cos^{-1}\left(2G_{\mathrm{R}} - 1\right) - n\pi\right\}. \quad (14)$$

By sweeping n and iterating calculations, it is possible to estimate the correct amount of the residual CD with $G_{\mathrm{R}} = 1$.

We conducted a WDM-amplification experiment for fundamental demonstration of this method. The setup was almost the same as that shown in Fig. 8. The 10-WDM CW were not modulated. Fig. 12 shows the PSA-stage configuration. Power measurements in PSA input and output were conducted by dividing the signal light with 1×2 couplers for simplicity. The BPF3 and BPF4 with 20-GHz bandwidth selectively extracted the components at f_{PLL} (193.1 THz) or f_{a} (193.2 THz). The measured power at f_{PLL} of input and output were -35.9 and -16.6 dBm, respectively. The measured power at f_{a} of input and output were -35.2 and -17.7 dBm, respectively. The G_{R} was calculated as 0.66, and the residual CD was estimated as 0.89 ps/nm. Fig. 13 shows the WDM spectrum with and without CD compensation. The gain variation of 15 dB was suppressed to less than 3 dB by CD compensation using the estimated CD. As a result, the fundamental operation of this method was confirmed.

In the above fundamental demonstration, the bandwidth of the BPFs for power measurements were set to a static 20 GHz. However, the measurement accuracy depends on the BPF bandwidth because the measured power depends on the measurement bandwidth. We numerically evaluated the estimation accuracy
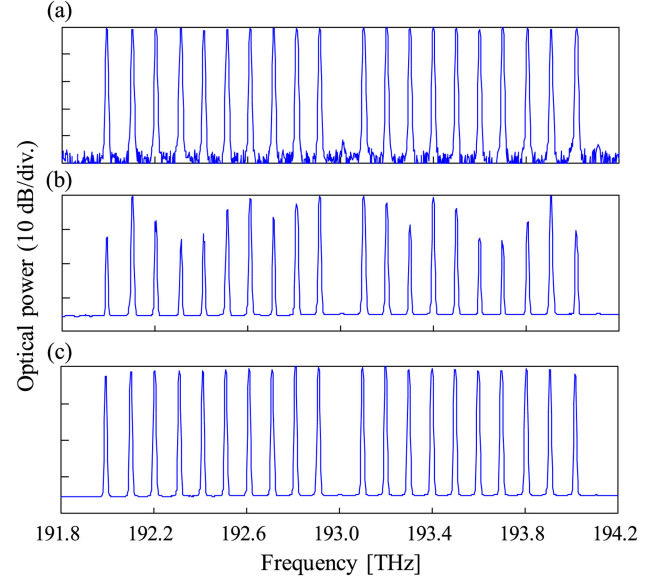

Fig. 13. Spectra of 10-WDM CW lights. (a) PSA-input spectrum. (b) Amplified spectrum without CD compensation. (c) Amplified spectrum with CD compensation using CD estimated from gain variation among channels.

dependence of this method on bandwidth of BPFs. The input light was assumed to have flat power without a gap in frequency. The amplified spectrum was calculated using Eq. (4) with 1-MHz resolution. The gain of the PSA was set to 20 dB, and the bandwidth of the BPFs were varied from 0.1 to 100 GHz every 0.1 GHz. The form of the BPFs passband was assumed as an ideal rectangle. The f_{PLL} was 193.1 THz, and f_{a} was varied from 193.2 to 194.0 THz in increments of 100 GHz assuming a 10-WDM channel with a 100-GHz grid. The CD estimations were carried out for residual CDs of 0.1, 0.5, and 0.9 ps/nm. Fig. 14 shows the simulation results of the error rate ε for each residual CD and f_{a}. The ε is expressed as

$$\varepsilon = \frac{|D_{\mathrm{T}} - D_{\mathrm{M}}|}{D_{\mathrm{T}}}, \quad (15)$$

where D_{T} and D_{M} indicate true and measured values, respectively. Non-plotted results for some f_{a} recorded an error rate larger than 5% due to the narrow measurement range. It was confirmed that estimation accuracy degraded along with the extension of BPF bandwidth. In the case of 0.1-ps/nm CD, the estimation with f_{a} larger than 193.8 THz exceeded measurement range calculated from Eq. (13), and the highest estimation accuracy was the case with $f_{\mathrm{a}} = 193.6$ THz. It was confirmed that the error rate is typically less than 1% when BPF bandwidth is narrower than 30 GHz. According to Eq. (4), it is expected that the compensation accuracy of about 0.01-ps/nm order is required for over 4-THz amplification bandwidth. If the residual CD is about 1 ps/nm, the BPF bandwidth should be selected to narrower than 30 GHz for the accuracy of 0.01-ps/nm order. The BPF bandwidth should be set in response to the amount of the residual CD and signal bandwidth.

Finally, we simulated a case in which the estimation target exceeds the measurement range. If the residual CD is greater than the measurement range, CD can be estimated by introducing the correction term of $n\pi$ according to Eq. (14) and sweeping n.
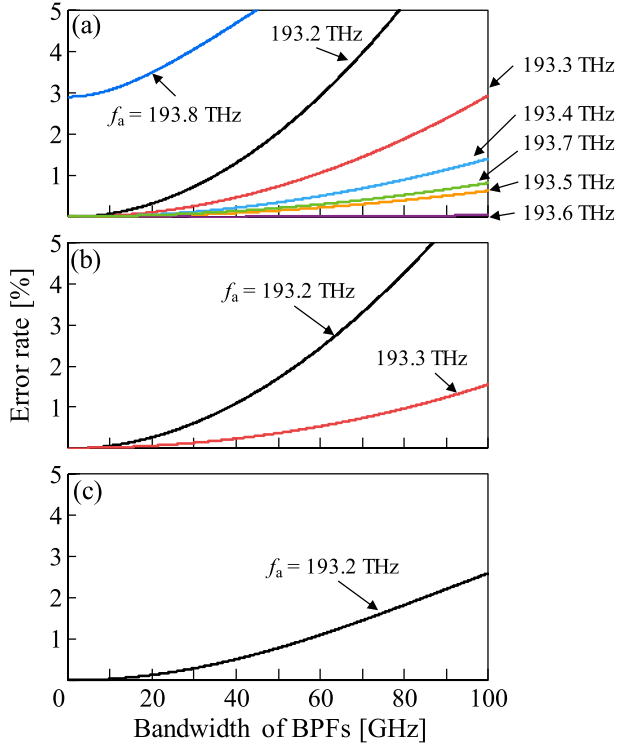
Fig. 14. Error rate as function of BPF bandwidth for each f_a for $f_{PLL} = 193.1$ THz. Estimation targets of residual CDs were (a) 0.1 ps/nm, (b) 0.5 ps/nm, and (c) 0.9 ps/nm.
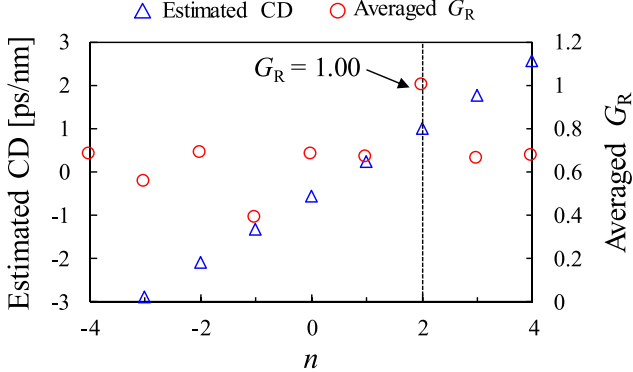

Fig. 15. Estimation CD values and averaged G_R after compensation with sweeping estimation. Given-residual CD was 1.00 ps-nm.

The CD corresponding to n when averaged G_R for some WDM channels after CD compensation becomes closest to 1 is the correct CD amount. We used this sweeping estimation under the same conditions as the simulation in the previous paragraph. The estimation target was 1.00-ps/nm CD with $f_a = 193.3$ THz. The bandwidths of the BPFs for power measurement were set to 10 GHz. Averaged G_R was calculated using each G_R between the channel at f_{PLL} and all other channels. Fig. 15 shows the estimated CDs and averaged G_R for each n. For $n = 0$, it was the CD exceeded measurement range because the averaged G_R after compensation was 0.68. The averaged G_R became closest to 1 when $n = 2$. The estimated CD with $n = 2$ was 1.00 ps/nm, which was in agreement with the true value. It was confirmed that correct residual CD can be estimated by sweep measurement even if the estimation target exceeds the measurement range.

The method using gain spectrum described in Section IV-A requires a broad ASE light for estimating CD, even though it provides stable estimation due to few parameters. On the other hand, the method using gain variation among WDM channels does not require the special test light and can operate in service. However, some parameters, such as BPF bandwidths and the correction term, need to be adjusted.

V. Conclusion

We investigated the impact of residual CD on ND-PSAs and proposed an accurate CD estimation method toward wideband phase-sensitive amplification.

We derived the theoretical gain-spectrum formula for ND-PSAs by modifying the conventional formula for D-PSAs, and the modified formula was experimentally validated using PPLN modules. To investigate the effect of the residual CD on signal quality, we also conducted amplification experiments of with 20- and 5-Gbaud PS-64QAM signals. The CD tolerance of the 5-Gbaud signal was higher than that of the 20-Gbaud signal due to passband narrowing, and the modified gain-spectrum formula properly described the passband of the ND-PSA.

We presented our proposed method for estimating residual CD from the measured gain spectrum and the modified theoretical formula. As a result, by compensating for the CD estimated by our method, residual CD was suppressed to less than 0.02 ps/nm, and gain-flatted spectrum over 3.5 THz was achieved. A 10-WDM amplification was demonstrated without signal deterioration using the gain-flatted PSA supported with this method. Moreover, we also proposed a method for estimating residual CD from the gain variation among WDM channels for monitoring and adaptively compensating for residual CD. We conducted an experiment to fundamentally demonstrate this method by amplifying 10-WDM CW lights, suggesting the possibility of adaptive compensation for residual CD. We evaluated the dependence of estimation accuracy of this method on bandwidths of BPFs used for measurement PSA gain through a numerical simulation. In addition, we indicated that residual CD can be estimated by sweep measurement even if the estimation target exceeds the measurement range.

References

[1] F. Hamaoka, "Ultra-wideband and broadband transmission technologies," in *Proc. Opt. Fiber Commun. Conf.*, Mar. 2020, Paper W3E.1.

[2] C. M. Caves, "Quantum limits on noise in linear amplifiers," *Phys. Rev. D*, vol. 26, no. 8, pp. 1817–1839, Aug. 1982.

[3] R. J. Essiambre and R. W. Tkach, "Capacity trends and limits of optical communication networks," *Proc. IEEE*, vol. 100, no. 5, pp. 1035–1055, May 2012.

[4] W. Imajuku, A. Takada, and Y. Yamabayashi, "Low-noise amplification under the 3-dB noise figure in a high gain phase-sensitive fiber amplifier," *Electron. Lett.*, vol. 35, no. 22, pp. 1954–1955, Oct. 1999.

[5] K. Croussore and G. Li, "Phase regeneration of NRZ-DPSK signals based on symmetric-pump phase-sensitive amplification," *IEEE Photon. Technol. Lett.*, vol. 19, no. 11, pp. 864–866, Jun. 2007.

[6] S. L. I. Olsson, B. Corcoran, C. Lundström, T. A. Eriksson, M. Karlsson, and P. A. Andrekson, "Phase-sensitive amplified transmission links for improved sensitivity and nonlinearity tolerance," *J. Lightw. Technol.*, vol. 33, no. 3, pp. 710–721, Nov. 2015.

[7] K. Vijayan, B. Foo, M. Karlsson, and P. A. Andrekson, "Cross-Phase Modulation Mitigation in Phase-Sensitive Amplifier Links," *IEEE Photon. Technol. Lett.*, vol. 31, no. 21, pp. 1733–1736, Sep. 2019.

[8] T. Umeki, O. Tadanaga, A. Takada, and M. Asobe, "Phase sensitive degenerate parametric amplification using directly-bonded PPLN ridge waveguides," *Opt. Express*, vol. 19, no. 7, pp. 6326–6332, Mar. 2011.

[9] B. J. Puttnam, D. Mazroa, S. Shinada, and N. Wada, "Phase-squeezing properties of non-degenerate PSAs using PPLN waveguides," *Opt. Express*, vol. 19, no. 26, pp. B131–B139, Nov. 2011.

[10] T. Torounidis, P. A. Andrekson, and B. -E. Olsson, "Fiber-optical parametric amplifier with 70-dB gain," *IEEE Photon. Technol. Lett.*, vol. 18, no. 10, pp. 1194–1196, May 2006.

[11] S. Takasaka *et al.*, "Quasi phase-matched FOPA with 50 nm gain bandwidth using dispersion stable highly nonlinear fiber," in *Proc. Opt. Fiber Commun. Conf.*, Mar. 2014, Paper W3E.2.

[12] R. Tang, P. S. Devgan, V. S. Grigoryan, P. Kumar, and M. Vasilyev, "In-line phase-sensitive amplification of multichannel CW signals based on frequency nondegenerate four-wave-mixing in fiber," *Opt. Express*, vol. 16, no. 12, pp. 9046–9053, Jun. 2008.

[13] T. Umeki, O. Tadanaga, M. Asobe, Y. Miyamoto, and H. Takenouchi, "First demonstration of higher-order QAM signal amplification in PPLN-based phase sensitive amplifier," *Opt. Express*, vol. 22, no. 3, pp. 2473–2482, Jan. 2014.

[14] Z. Tong *et al.*, "Towards ultrasensitive optical links enabled by low-noise phase-sensitive amplifiers," *Nat. Photon.*, vol. 5, no. 7, pp. 430–436, Jul. 2011.

[15] T. Umeki *et al.*, "Polarization-diversity in-line phase sensitive amplifier for simultaneous amplification of fiber-transmitted WDM PDM-16QAM signals," in *Proc. Opt. Fiber Commun. Conf.*, Mar. 2018, Paper M3E.4.

[16] Y. Akasaka *et al.*, "WDM amplification of one pump HNLF based phase sensitive amplifier with static pump phase tuning," in *Proc. Opt. Fiber Commun. Conf.*, Mar. 2019, Paper W4F.5.

[17] S. L. I. Olsson, H. Eliasson, E. Astra, M. Karlsson, and P. A. Andrekson, "Long-haul optical transmission link using low-noise phase-sensitive amplifiers," *Nat. Commun.*, vol. 9, Jun. 2018, Art. no. 2513.

[18] M. Asobe, T. Umeki, K. Enbutsu, O. Tadanaga, and H. Takenouchi, "Phase squeezing and dispersion tolerance of phase sensitive amplifier using periodically poled LiNbO3 waveguide," *J. Opt. Soc. Amer. B*, vol. 31, no. 12, pp. 3164–3169, Dec. 2014.

[19] Y. Akasaka *et al.*, "Study of chromatic dispersion effect on 16QAM phase sensitive amplification," in *Proc. IEEE Photon. Conf.*, Oct. 2015, Paper WG1.1.

[20] S. Shimizu *et al.*, "Gain ripple and passband narrowing due to residual chromatic dispersion in non-degenerate phase-sensitive amplifiers," in *Proc. Opt. Fiber Commun. Conf.*, Mar. 2020, Paper M1I.3.

[21] W. Imajuku and A. Takada, "Noise figure of phase-sensitive parametric amplifier using a Mach–Zehnder interferometer with lossy Kerr media and noisy pump," *IEEE J. Quantum Electron.*, vol. 39, no. 6, pp. 799–812, Jun. 2003.

[22] T. Kazama, T. Umeki, M. Abe, K. Enbutsu, Y. Miyamoto, and H. Takenouchi, "Low-parametric-crosstalk phase-sensitive amplifier for guardband-less DWDM signal using PPLN waveguides," *J. Lightw. Technol.*, vol. 35, no. 4, pp. 755–761, Aug. 2016.

[23] Y. Okamura *et al.*, "Optical pump phase locking to a carrier wave extracted from phase-conjugated twin waves for phase-sensitive optical amplifier repeaters," *Opt. Express*, vol. 24, no. 23, pp. 26300–26306, Nov. 2016.

[24] T. Kato, Y. Koyano, and M. Nishimura, "Temperature dependence of chromatic dispersion in various types of optical fiber," *Opt. Lett.*, vol. 25, no. 16, pp. 1156–1158, Aug. 2000.

Shimpei Shimizu (Member, IEEE) received the B.E. degree in engineering and the M.E. degree in information science and technology in the field of electronics for informatics from Hokkaido University, Sapporo, Japan, in 2016 and 2018, respectively. In 2018, he joined NTT Network Innovation Laboratories, Yokosuka, Japan. His current research interest is high-capacity optical transmission systems. He is a member of the Institute of Electronics, Information and Communication Engineers (IEICE) of Japan and the IEEE Photonics Society. He was the recipient of the 2017 IEICE Communications Society Optical Communication Systems Young Researchers Award.

Takushi Kazama received the B.S. and M.S. degrees in electrical engineering from The University of Tokyo, Tokyo, Japan, in 2009 and 2011, respectively. In 2011, he joined NTT Device Technology Laboratories, Japan, where he has been engaged in research on nonlinear optical devices based on periodically poled LiNbO$_3$ waveguides. He is a member of the Institute of Electronics, Information, and Communication Engineers of Japan (IEICE) and the Japan Society of Applied Physics (JSAP).

Takayuki Kobayashi (Member, IEEE) received the B.E., M.E., and Dr. Eng. degrees from Waseda University, Tokyo, Japan, in 2004, 2006, and 2019, respectively. In 2006, he joined NTT Network Innovation Laboratories, Yokosuka, Japan, where he was engaged in the research on high-speed and high-capacity digital coherent transmission systems. In 2014, he moved to NTT Access Network Service Systems Laboratories, Yokosuka, and was engaged in 5G mobile optical network systems. In 2016, he moved back to NTT Network Innovation Laboratories and has been working on high-capacity optical transmission systems. His current research interests are long-haul optical transmission systems employing spectrally efficient modulation formats enhanced by digital and optical signal processing. He is a member of the Institute of Electronics, Information and Communication Engineers (IEICE) of Japan. He has served as a Technical Program Committee (TPC) Member of the Electrical Subsystems' Category for the Optical Fiber Communication Conference (OFC) from 2016 to 2018. He has been serving as a TPC Member of the "Point-to-Point Optical Transmission" Category for the European Conference on Optical Communication (ECOC) since 2018.

Takeshi Umeki (Member, IEEE) received the B.S. degree in physics from Gakusyuin University, Tokyo, Japan, in 2002, the M.S. degree in physics, and the Ph.D. degree in nonlinear optics from The University of Tokyo, Tokyo, in 2004 and 2014, respectively. He joined NTT Photonics Laboratories, Atsugi, Japan, in 2004, since then he has been involved in research on nonlinear optical devices based on periodically poled LiNbO$_3$ waveguides. He is a member of the Japan Society of Applied Physics (JSAP), the Institute of Electronics, Information, and Communication Engineers (IEICE), and the IEEE/Photonics Society.

Koji Enbutsu received the B.E. and M.E. degrees in electronics engineering from Hokkaido University, Sapporo, Japan, in 1994 and 1996, respectively. In 1996, he joined NTT Opto-Electronics Laboratories, Japan, where he was engaged in research on organic optical waveguides for optical communications and electro-optic crystals and their devices. In 2007, he moved to the NTT Access Services Network System Laboratories, where he was engaged in research on optical fiber testing and monitoring. He is a member of the Institute of Electronics, Information, and Communication Engineers (IEICE) and the Japan Society of Applied Physics (JSAP).

Ryoichi Kasahara received the B.S. degree from The University of Electro-Communications, Tokyo, Japan, in 1995 and the M.S. degree from Tohoku University, Sendai, Japan, in 1997. In 1997, he joined NTT Opto-Electronics Laboratories, Japan, where he was involved in research on silica-based planar lightwave circuits (PLCs), including thermo-optic switches, arrayed-waveguide grating multiplexers, and integrated optoelectrical receiver modules. He is currently with NTT Device Technology Laboratories, Japan, where he has been involved in the research and development of the fabrication technologies of optical dielectric waveguide devices. He is a Senior Member of the Institute of Electronics, Information, and Communication Engineers of Japan (IEICE) and a member of the Japan Society of Applied Physics (JSAP).

Yutaka Miyamoto (Member, IEEE) received the B.E. and M.E. degrees in electrical engineering from Waseda University, Tokyo, Japan, in 1986 and 1988, respectively, and the Dr. Eng. degree in electrical engineering from Tokyo University, Tokyo, in 2016. He joined NTT Transmission Systems Laboratories, Yokosuka, Japan, in 1988, where he was engaged in the research and development of highspeed optical communications systems including the 10-Gbit/s first terrestrial optical transmission system (FA-10G) using erbium-doped fiber amplifiers (EDFA) inline repeaters. He was with NTT Electronics Technology Corporation, Yokohama, Japan, from 1995 to 1997, where he was engaged in the planning and product development of high-speed optical module at the data rate of 10 Gb/s and beyond. Since 1997, he has been with NTT Network Innovation Laboratories, Yokosuka, where he has contributed to the research and development of optical transport technologies based on 40/100/400-Gbit/s channel and beyond. He is currently an NTT Fellow and the Director of the Innovative Photonic Network Research Center, NTT Network Innovation Laboratories, where he has been investigating and promoting the future scalable optical transport network with the Pbit/s-class capacity based on innovative transport technologies such as digital signal processing, space division multiplexing, and cutting-edge integrated devices for photonic preprocessing. He is a fellow of the Institute of Electronics, Information and Communication Engineers (IEICE).